SAVIAC Proceedings 66th Shock and Vibrations Symposium, Biloxi, MS, Vol.2, pp265-276, November 1995

SPARK-GENERATED BUBBLES AS LABORATORY-SCALE MODELS OF UNDERWATER EXPLOSIONS AND THEIR USE FOR VALIDATION OF SIMULATION TOOLS

G.L Chahine*, G.S. Frederick*, C.J. Lambrecht*
G.S. Harris**, H.U. Mair**

*DYNAFLOW, INC.
7210 Pindell School Road, Fulton, MD 20759
www.dynaflow-inc.com

**Naval Surface Warfare Center,
Indian Head Division, Code 460
Silver Spring, MD 20903-5640

Spark-generated bubbles are strong candidates for laboratory-scale models of underwater explosion (UNDEX) bubble dynamics and are, therefore, excellent sources of data for validation of simulation tools. Their relative safety, cleanliness and compactness enable high quality observations of bubble dynamics at relatively low cost compared to experiments involving explosives. This document addresses the relevant advantages of spark-generated bubbles, focusing on re-entrant jet visualization. It also addresses scaling issues and concerns about the deposition of energy into the bubble as a result of the electric discharge process. In conclusion, a procedure is specified for using spark-generated bubbles as laboratory-scale models of UNDEX bubble dynamics and as data for validation of simulation tools.

INTRODUCTION

Spark generators have been used for studying bubbles in a liquid for quite a long time [1,2,3,4]. The use of high speed cameras to photograph spark-generated bubbles produces high quality observations of bubble dynamics including clear visualization of reentrant jet formation inside the bubble. Since one of the primary unsolved problems in the study of explosion bubble dynamics is the clear elucidation of the hydrodynamic phenomena accompanying and following 'touchdown' of the re-entrant jet, such observations can be extremely useful in developing and validating numerical models.

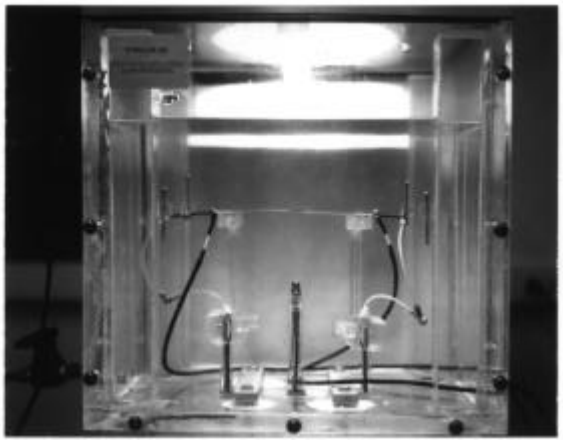

Figure 1. Photograph of Spark Bubble Test Tank

Figure 2. Bubble dynamics in a gravity field showing reentrant jet dynamics and toroidal bubble rebound.

Use of a vacuum pump to lower the ambient pressure in a Plexiglas tank (see *Figure 1*) and a high voltage to generate the spark enables one to create bubbles of sizes of the order of one inch in diameter possessing periods of oscillation of the order of ten milliseconds. As a result, with a 10,000 frames per second (or 40,000 quarter-frames per second) high speed camera equipped with a conventional lens, one is able to obtain a clear and precise record of the bubble dynamics. As illustrated in *Figures 2, 3,* and *4*, the pictures obtained allow one to clearly follow the bubble dynamics and the interface motion, including the motion and penetration of the reentrant jet through the bubble interior and back into the fluid [5].

Experimentation with spark-generated bubbles removes several disadvantages associated with experimentation using explosives. First, the use of explosives incurs the expenses of performing the actual tests, both in the field and in laboratory settings, as well as the expense, time consumption and "red tape" associated with explosive safety precautions. Moreover, the explosive detonation products generally occlude the view of the interior of the bubble, and do not allow visualization of the details of the formation of the jet, the touchdown and the ensuing behavior.

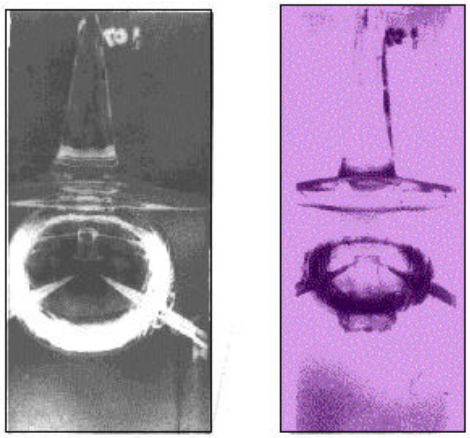

Figure 3. Re-entrant jet in a bubble near a free surface showing upward plume and downward jet.

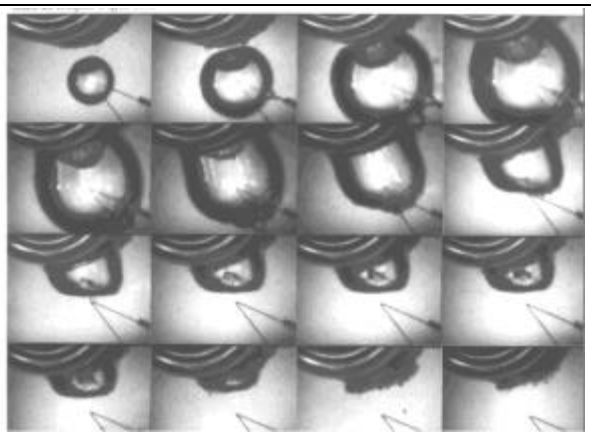

Figure 4. Bubble interaction with a flexible cylinder.

However, despite their more complex nature, explosively-generated bubbles possess the advantage of significant, sustained, and well documented efforts devoted to their study. This has resulted in well verified scaling laws [6,7,8,9] based on testing and observation. Spark generators, on the other hand, have been used in only a few laboratories, mostly for fundamental cavitation bubble dynamics studies, and their practical use has been rather poorly documented.

Spark generators were often used to obtain a *qualitative* understanding of the nature of bubble dynamics as opposed to a *quantitative* one. Thus, an important question here that was seldom asked in these studies is:

- For a given ambient pressure in the test tank, and for a given amount of input energy in the condenser, what are the maximum radius, R_{max}, minimum radius, R_{min}, and period of oscillation, T, of the generated bubble?

This question is, in fact, difficult to answer due to the significant energy losses associated with the spark process. Experimental studies show that less than 15 percent of the energy stored in the condenser goes into the bubble [2]. As a result, without actual experimental observation, a potentially large error exists on the estimation of the energy actually deposited in the bubble. In practice, the losses depend on the particular set-up, the water quality, and the nature and, to a lesser extent, spacing of the electrodes.

However, as we will see below, experimentation enables one to respond more easily to a related question, which is as useful for our purpose here. That is:

- For a given set of experimental conditions, and using the observation of the time history of the bubble growth and collapse, can one determine the bubble conditions needed to start a numerical computation, i.e. can one deduce the initial bubble radius, R_o, radial velocity, $\dot{R}_0$, and gas pressure, P_{go}?

The advantage of posing the problem this way is that it makes the proposed method independent of the particular experimental set-up or spark generator used. In fact, as demonstrated below, the proposed method is relatively insensitive to the way the bubble is generated as long as its dynamics are controlled by fluid dynamic effects, as opposed to heat, mass transfer, or other interfacial effects.

In this study, we use experimental data and the approach described below to determine the three key parameters necessary for Computational Fluid Dynamics (CFD) computations: R_{max}, R_{min} and P_{go}. For simulations that include the description of the explosive detonation process, we can also provide conditions (i.e., charge weight and depth) with equivalent TNT charges. We will see below that the values so obtained enable one to theoretically "predict" a bubble history, which *qualitatively* and *quantitatively*, differs little from observed results.

BACKGROUND

Energy Deposition

The underwater spark is a process by which electrical energy is converted into a small volume plasma which has temperatures as high as 20,000 degrees K, and pressures as high as 10,000 atmospheres [2]. As the trigger pulse breaks down the hold-off gap between electrodes, current flows between the electrodes, with energy being absorbed in the plasma at a rate depending upon the power input and the inertia of the water. Eventually, due to a decrease in the voltage and an increase in the ionization, temperature, and pressure of the plasma, the spark is extinguished. The energy is initially stored in the plasma in the form of dissociation, excitation, ionization, and kinetic energy of the constituent particles.

While the heated and pressurized plasma will tend to expand, the inertia of the outside water will tend to confine it. Mechanical work, light radiation, thermal radiation, and thermal conduction dissipate the energy from the plasma at a rate slower than energy input from the spark. Because of the high pressure, the liquid near the plasma interface is initially compressed. This high pressure leads to the formation of a shock wave that radiates outward. The energy in the shock wave comprises 20 to 50 percent of the energy imparted by the spark into the water [2]**.** After emission of the shock wave, the pressure in the gas sphere quickly falls, but remains well above that of the surrounding liquid. The pressure difference, however, is small enough that compressible effects can be neglected. From this point on, incompressible hydrodynamic effects dominate, and this process can be simulated by incompressible CFD codes. The pressurized gas expands into a large bubble which subsequently collapses and re-expands.

The phenomena preceding the incompressible hydrodynamic phase occur quickly and are accompanied by light generation that prevents accurate determination of the initial bubble radius using conventional high-speed photography. To model the growth and collapse of the bubble using incompressible CFD codes, consistent initial conditions (R_o and P_{go}) are required, and the object of our present study is to establish these conditions for particular experiments. Here R_o and P_{go} correspond to initial conditions at the start of the incompressible hydrodynamic phase. To this end, we consider first the theory of spherical bubble dynamics.

Free Field Bubble Observations

As it is for underwater explosion bubble studies, it is essential to first characterize spark-generated bubble behavior far away from any boundaries, and in the absence of significant gravity effects. Tests conducted at higher ambient pressure result in a smaller effect of gravity or, correspondingly, a larger value of the Froude number, F [5]:

$$F = \frac{P_{amb}}{2\,rgR_{\max}} = \frac{P_{cell} + rgZ}{2\rho gR_{\max}}, \tag{1}$$

where Z is the distance between the electrode gap and the test cell free surface, and P_{cell} is the imposed pressure at the free surface in the test cell. Test conducted at higher values of P_{cell} affect F not only through the numerator in Equation (1), but also through R_{max} in the denominator, which becomes smaller for higher values of P_{cell}.

Table 1 shows the characteristics of the bubbles used in the analysis below. These were obtained from various experiments [4,10,11] by analyzing high-speed movies of fifteen free field, nearly spherical bubbles. The ambient conditions in these experiments were varied significantly, from 0.05 atm up to 0.75 atm (a 15-fold variation) resulting in bubble sizes between 12.6 mm and 2.7 mm. *Figure 6* shows bubble radius versus time for all cases of *Table 1* using dimensional variables.

Table 1. Characteristics of the spark-generated bubbles used in the observations

RUN No.	R_{max} (mm)	T (ms)	P (mmHg)
PY 7	12.6	6.91	102
PY 8	6.5	1.59	349
PY 9	5.5	1.16	561
PY 14	7.2	4.88	78
PY 15	7.3	5.71	38
PY 18	2.7	0.83	312
PY 19	4.5	1.45	312
PY 21	3.8	0.92	567
PY 22	4.3	1.18	570
PY 32	5.1	1.06	570
PY33	7.2	1.85	314
PY 34	7.5	2.04	314
PY 35	10.4	4.38	108
PY 36	10.6	5.30	108
DF 920603	29	40.98	24

In order to compare these various cases, the theory of spherical bubble dynamics discussed below is invoked. From a practical viewpoint, since there is some uncertainty in the zero of the curves due to the timing between frames and the presence of a bright spot on the film following sparking, we have adopted the following normalization. Lengths are normalized by R_{max}, as is usually done for underwater explosion bubbles. Times are normalized by the time needed for the bubble to grow from 0.6 R_{max} up to R_{max} then come back down to 0.6 R_{max}. This time, called $T_{60\%}$, was chosen based on previous analyses of bubble films [4,11].

Figure 5 shows the normalized data. As can be seen, this results in good correlation of all bubble radius histories, independent of the generator and the electrodes. In fact, *Figure 5* is a characteristic spark-generated spherical bubble radius history for ambient pressure conditions that are significantly higher than the water vapor pressure. It would, therefore, be desirable to determine if it fits classical bubble dynamics and explosion bubble theories.

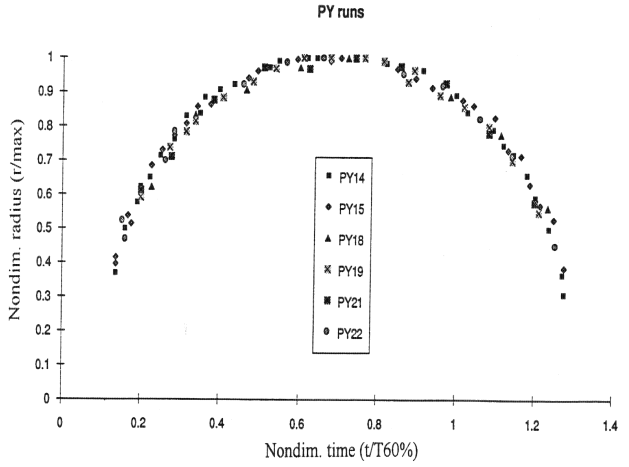

Figure 5. Normalized bubble radius versus time for the cases shown in Figure 5.

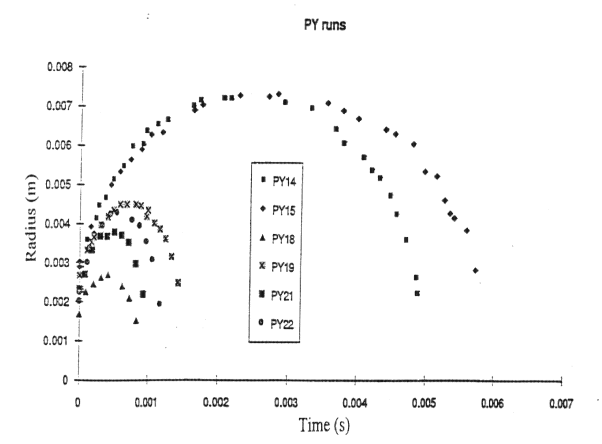

Figure 6. Bubble radius versus time for selected cases of Table 1.

REVIEW OF BUBBLE THEORY

Spherical Bubble Dynamics Theory

As is generally done for underwater explosion bubbles, let us start by characterizing the explosion bubbles in deep free-field conditions; that is, when the bubble and its subsequent dynamics possess spherical symmetry, and when dynamic forces are predominant over heat and mass transfer effects. In that case, as described in more detail in [5], the bubble-water interface can be described by $r = R(t)$. At every instant, a balance between the pressure in the liquid at the point M on the surface, $P_l(M)$, and the pressure inside the bubble and surface tension exists, and can be written as:

$$P_l(M) = P_v + P_{go}\left(\frac{V_o}{V}\right)^k - C s \tag{2}$$

where σ the surface tension at the liquid-bubble interface, V the instantaneous bubble volume, V_o its initial value, and C is the local curvature of the bubble. The pressure inside the bubble is decomposed into two partial pressures: P_v , the liquid vapor pressure at the ambient temperature, and the gas pressure, P_g , which is related to a reference value P_{go} at volume V_o by a polytropic compression law

$$P_g V^k = P_{go} V_o^k \tag{3}$$

The constant k is between 1.0 (isothermal) and C_p/C_v (adiabatic)[1] and V_o and V are the reference and instantaneous values of the bubble volume, respectively.

The dynamics of a spherical explosion bubble generated at an ambient pressure P_a is given by the following governing equation, [5]:

$$r\left[R\ddot{R} + \frac{3}{2}\dot{R}^2\right] = P_{go}\left(\frac{R_o}{R}\right)^{3k} + P_v - P_a - \frac{2s}{R} \tag{4}$$

where P_a is the ambient pressure at the bubble center level, and dots denote time derivatives. This equation is termed the Rayleigh-Plesset equation, and when integrated, subject to appropriate initial conditions discussed further below, gives the bubble radius versus time.

When the ambient pressure, P_a, is constant, Equation (4) is integrable and for polytropic behavior $k \neq 1$, [5]) becomes:

$$\dot{R}^2 = \frac{2}{r}\left[\frac{P_g}{3(1-k)}\left(1-e^{3k-3}\right) + \frac{P_v - P_a}{3}\left(1-e^{-3}\right) - \frac{s}{R}\left(1-e^{-2}\right)\right] \tag{5}$$

where

$$e = \frac{R}{R_{\max}} \tag{6}$$

and the gas compression law,

$$P_g R^{3k} = P_{go} R_o^{3k} \tag{7}$$

has been used. At maximum and minimum bubble radius, $\dot{R} = 0$; as a result, using equation (5), the following relation between P_{go}, R_o and R_{max} is obtained:

$$P_{go} = \frac{3(1-k)}{1-e_o^{3k-3}}\left[\frac{P_a - P_v}{3}\left(1-e_o^{-3}\right) + \frac{s}{R}\left(1-e_o^{-2}\right)\right] \tag{8}$$

with

$$e_o = \frac{R_{\min}}{R_{\max}} = \frac{R_o}{R_{\max}} \tag{9}$$

[1] For monatomic, di-atomic, and tri-atomic gases C_p/C_v is 1.667, 1.4, and 1.333 respectively.

Inclusion of Heat and Mass Transfer Effects

Mass and heat transfer effects at the bubble/liquid interface occur due to evaporation, condensation, and dissolution of explosion products at the interface of the superheated liquid. These phenomena, especially heat transfer due to local superheated water boiling, are usually negligible for deep water explosions but may become important in shallow water explosions and for spark-generated bubbles at very low ambient pressures [12,13,14]. In the dynamic equations discussed above, e.g. in the balance of pressures at the bubble interface, these effects are expressed by the fact that the vapor pressure term in the pressure balance equation at the bubble/liquid interface becomes time dependent since the actual temperature at the bubble wall is then a strong function of time.

These heat transfer effects can be incorporated in the Rayleigh-Plesset formulation. To do this, one has to add the energy equation in the liquid to the dynamics equations of the system:

$$\frac{dT}{dt} + \nabla f \bullet \nabla T = \mathsf{D}\nabla^2 T \tag{10}$$

subject to the following boundary condition:

$$K \iint \left.\frac{dT}{dn}\right|_{r=R(q,f,t)} R^2(q,f,t)\sin q\, dq\, df = r_v \mathsf{L} \frac{d}{dt}\left[\iint \frac{R^3(q,f,t)}{3}\sin q\, dq\, df\right] \tag{11}$$

where T is the temperature in the liquid, D is the liquid thermal diffusivity, r_v is the water vapor density, L is the latent heat of vaporization of the liquid, and K the liquid thermal conductivity. Equation (11) states that the heat locally lost at any point of the bubble boundary is used to vaporize an amount of liquid determined by the local bubble-volume expansion rate. A similar equation can be written to account for the gas expansion/compression during the bubble growth/collapse [15]. Equation (11) is satisfied if the following equilibrium equation applies locally at the bubble interface:

$$\left.\frac{\partial T}{\partial n^i}\right|_{r=R^i(q,f,t)} = \frac{r_v \mathsf{L}}{k}\dot{R} \tag{12}$$

Equations similar to these in [12,15] have been developed to study gas diffusion and heat exchange in and out of the bubbles.

For the study of the heat problem it is useful to introduce the following variable (omitting the superscripts i):

$$y = \frac{1}{3}\left[r^3 - R^3(q,f,t)\right] \tag{13}$$

With this variable change, the normalized energy equation can be written:

$$\dot{T} + \frac{\partial T}{\partial y}\left[r^2\frac{\partial \Phi}{\partial r} - R^2\dot{R}\right] = \mathsf{P}_e^{-1}\frac{\partial}{\partial y}\left(r^4\frac{\partial T}{\partial y}\right) + \frac{\mathsf{P}_e^{-1}}{r^2\sin q}\left[\frac{\partial}{\partial q}\left(\sin q\frac{\partial T}{\partial q}\right) - \frac{\partial}{\partial q}\left(R^2\frac{\partial R}{\partial q}\sin q\frac{\partial T}{\partial y}\right)\right] \tag{14}$$

After replacing R by its value derived from (4), we obtain the relation:

$$\dot{T} - \mathsf{P}_e^{-1}\frac{\partial}{\partial y}\left(h^4\frac{\partial T}{\partial y}\right) = 0. \tag{15}$$

where $h = \left(a_o^3 + 3y\right)^{1/3}$, and the Péclet number, $\mathrm{P_e}$, is the ratio of the thermal diffusion time $R_{\max}^2 / D$ to the bubble characteristic time τ,

$$\mathrm{P}_e = R_{\max}^2 / D t_o. \tag{16}$$

Similarly, the heat-balance condition on the bubble wall becomes:

$$R^2 \frac{\partial T}{\partial y}\bigg|_{y=0} = \mathrm{A} R \dot{R}, \tag{17}$$

where A characterizes the degree of superheat, and is given by the Jacob number:

$$\mathrm{A} = \frac{\rho_v L r_{b0}^2}{K t_0 \left(T_\infty - T_b\right)}, \tag{18}$$

T_b is the boiling temperature at the ambient pressure and T_∞ is the ambient temperature, therefore $\left(T_\infty - T_b\right)$ is the amount of superheat.

These equations can be integrated numerically in a manner similar to the Rayleigh-Plesset equation.

COMPARISON OF OBSERVATIONS WITH THEORY

Free Field Bubbles

In order to compare the experimental results with theoretical predictions, let us consider the Rayleigh-Plesset equation for spherical bubble dynamics described in the previous section. The key difficulty in using this equation is similar to that faced in answering the two questions raised in Section 1. In order to solve the second order ordinary differential Rayleigh Plesset equation we need two initial conditions on the radius, i.e. *R(0)* and $\dot{R}(0)$. One also needs to know the forcing terms such as the ambient pressure, the surface tension, and the initial gas pressure, P_{go}. In addition, parameters in the compression law for the gas in the bubble, e.g. the value of the polytropic constant *k*, are required. The four quantities *R(0)*, $\dot{R}(0)$, P_{go} and *k* are difficult to obtain directly from the analysis of a high speed movie of the phenomenon. Our aim here is to establish procedures that enable us to deduce these quantities from other quantities that are more easily measurable.

Using a numerical integration of the Rayleigh-Plesset equation, the bubble period and the maximum bubble radius were used to search for a match with the experimental data. This program was run using the *unknown* initial conditions *R(0)*, $\dot{R}(0) = 0$, and P_{go} as *variable* input that was varied until the simulation achieved a good match for both $R_{\max}$ and the bubble period. For the runs for which a match was available, the radius versus time curve given by the Rayleigh-Plesset equation was compared with the observed time histories.

For all runs at relatively high ambient pressures where "boiling" effects are absent or negligible, a set of initial conditions for each value of *k* could be found for the Rayleigh-Plesset equation which matched the experimental data. For these runs, it was found that a match was possible for any value of the gas constant *k* in the range *1<k<5/3*, i.e., an initial radius could be found to produce a theoretical curve that matched the known maximum radius and bubble period for any value of *k* in this range.

The experiments performed at very low ambient pressures (where heat transfer effects cannot be neglected) could, however, not be matched with the Rayleigh-Plesset equation, i.e. no initial radius for any value of the gas constant could be found to produce an appropriate time history. We attribute this to the fact that at these very low pressures, the vapor pressure is a significant portion of the total pressure inside the bubble during a significant period of its life. This makes vapor-transport effects important, an effect that is not included in the Rayleigh-Plesset equation. When required, these effects can be included to improve the fit.

To summarize, the algorithm for matching the experiment and theory is:

1) Obtain high speed movie of bubble history for a prescribed ambient pressure,

2) Find the maximum radius by frame-by-frame examination of the movie,
3) Find the time to maximum bubble radius and to collapse (minimum radius),
4) Iterate the Rayleigh-Plesset integration routine to find possible initial bubble radii which fit constraints of known maximum radius and known period for a given *k*. Determine corresponding initial gas pressure,
5) Compare radius-time curve to time history of bubble movie for the conditions that match,
6) Determine the value of *k* that gives the best fit.

Figure 7 shows the results of calculations using a set of *R(0)* and *k* values that achieves a specified value of the bubble period for a given value of Amax. This graph clearly indicates the importance of the knowledge of K. By comparing these calculations to the measured data, a value of *k* of 1.4 was found to produce the best fit, as shown in Figure 8. This result suggests that the gas in the spark-generated bubble is composed of a diatomic gas, which is consistent with the presence of dissociated water (H_2 and O_2) generated by the spark discharge. It is important to note that this is a non-condensable permanent gas, <u>not</u> water vapor. Had the gas within the bubble behaved like water vapor (i.e., a condensable gas), the resulting K would have been zero. The presence of a permanent gas with a *k* on the order of 1.4 compares favorably with the behavior of explosive gas products, which have *k*'s in the range of 1.25 to 1.4 [9].

Bubble Dynamics Near Structures/Walls

Near the wall, and in the absence of repeated controlled experiments, there was some uncertainty about the value of the maximum bubble radius measured from the experiment. This is a result of the lack of spherical bubble experiments (i.e., free field) at corresponding conditions. Consequently, the nondimensional distance to the solid wall had to be approximated within the range of experimental uncertainty to achieve a good fit of theory to experiment. Figure 9 and Figure 10 present the measured and computed time histories of the point on the bubble surface that lies along the axis of symmetry at the point originally farthest from the wall. This point is at the tip of the reentrant jet. A satisfactory match is observed. Note that the experiments include tests with nondimensional standoffs that are smaller and larger than one. This capability of spark bubble testing is especially important, since experimental data for the closer standoffs are needed to guide numerical model development for many cases of practical interest.

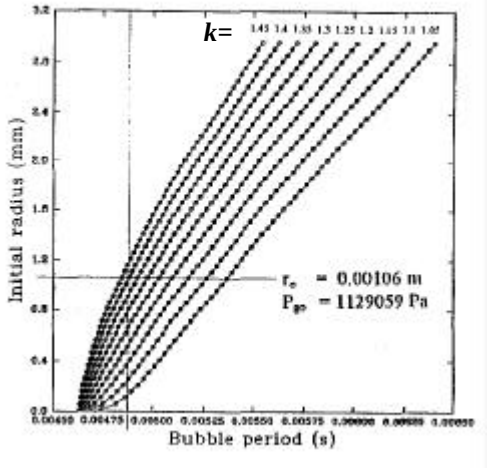

Figure 7. Example of the possible set of $R_\circ$ and k values to achieve a specified value of the period for a given value of R_{max}.

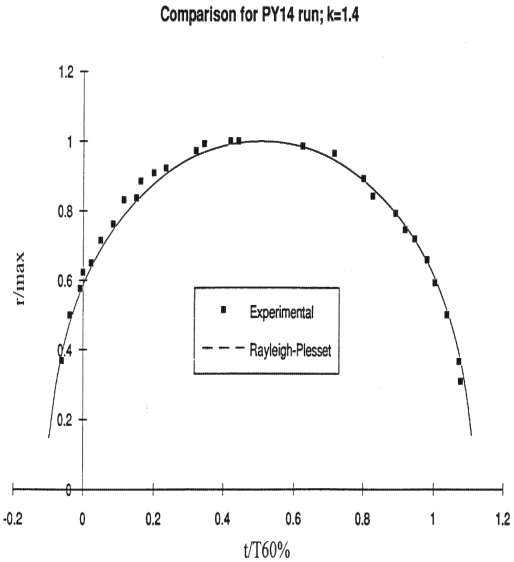

Figure 8. Comparison between experimental values of the Rayleigh-Plesset equation. And a solution for k=1.4.

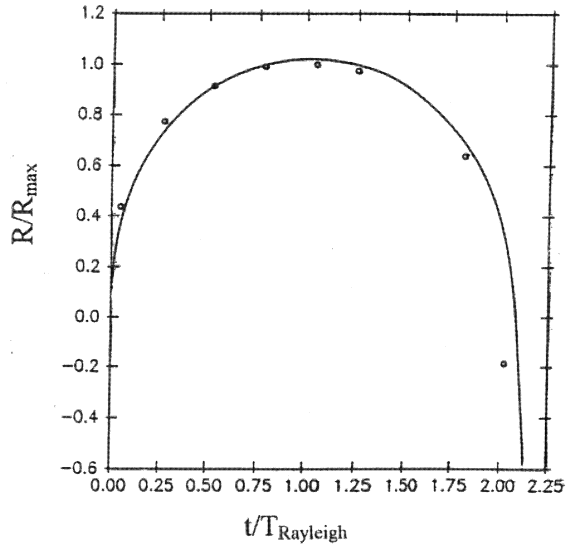

Figure 9. Time history of the re-entrant jet tip for a bubble collapsing onto a wall for $l/R_{max}=0.7$

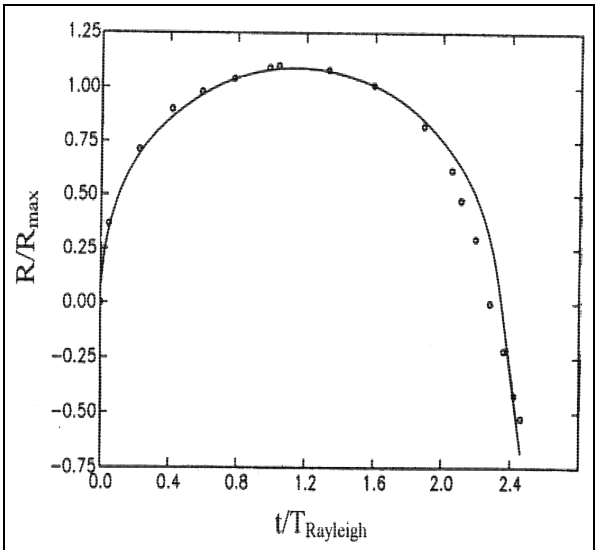

Figure 10. Time history of the re-entrant jet tip for a bubble collapsing onto a wall for $l/R_{max}=1.8$

Matching of Bubble Initial Conditions With Explosives Characteristics

Snay, *et al* [6,8] and Goertner, *et al*, [9] as well as earlier scientists [7], have experimentally and theoretically analyzed the behavior of explosion bubbles. Relationships between bubble period, bubble maximum radius, minimum to maximum size ratio, and the charge weight and its depth were derived. The knowledge of these characteristic dimensions are usually used to determine the values of the reference scales for the phenomenon. We propose here to use them as an intermediary link to obtain the explosive weight of TNT corresponding to the spark-generated bubble. To do so we need a correspondence between the determination of the initial bubble characteristics ($R(0)$, $\dot{R}(0)$, P_{go} and k) and the explosive (TNT) weight and depth conditions. For instance, the bubble period, T (in seconds), is related to the charge weight, W (in pounds), and to the hydrostatic head, Z (in feet of water), by the relation:

$$T=K\,W^{1/3}\,Z^{-5/6} \tag{19}$$

The period coefficient K is a characteristic of the explosive composition (e.g., 3.22 for lead azide and 4.25 for TNT). The maximum radius, R_{max} (in feet), is also related to Z, W, and the radius coefficient, J, by the relation:

$$R_{max}=J(W/Z)^{1/3}, \tag{20}$$

(J is about 9.2 for lead azide and 13.1 for TNT). The size ratio is also a characteristic of the explosive composition and is given by the constant e, ($e \cong 0.022$ for TNT and 0.026 for lead azide)

$$R_{min}/R_{max}=eZ^{1/3}. \tag{21}$$

Therefore, knowing T, $R_o=R_{min}$, R_{max}, and the TNT characteristics, J, e and K, the corresponding explosive weight and depth can be determined.

SUMMARY

- Analysis of experimental data from spark-generated bubbles shows that the bubble dynamics can be described by a characteristic bubble radius history using non-dimensionalized parameters.
- From the experimental data, characteristic initial conditions of bubble size and initial internal pressure can be determined to link the experimental data to theoretical models.
- Using an iterative procedure, experimental data from spark-generated bubbles was compared to classical spherical bubble dynamics theory to establish the internal gas constant, k, which matches the radius-time curve observed in the experiments. [A value of $k = 1.4$ was found to produce the best fit.]
- A value of k = 1.4 suggests the presence of diatomic gas. This is consistent with the presence of dissociated water (H2 and O2) which behaves like a permanent, non-condensable gas.
- Evaluation of the gas constant for the spark generated bubbles (k=1.4 showed that the gross gas properties were similar to the gas properties of explosion bubbles, where k ranges between 1.25 and 1.4.
- A procedure was described to link the spark bubble characteristics to equivalent explosion bubble conditions.
- The successful link of the spark bubble data to spherical bubble theory and to equivalent explosive conditions provides a firm foundation for the use of spark-generated bubbles to model full-scale explosion bubble dynamics.

In order to scale a full-scale explosion bubble in the spark chamber, the primary scaling parameter is the Froude Number, which is appropriate for fluid dynamics that are strongly influenced by gravity effects.

ACKNOWLEDGEMENTS

This work was partially supported by the Mechanics & Energy Conversion, Science and Technology Division of the Office of Naval Research.

REFERENCES

[1] Ellis, A. T., "Parameters Affecting Cavitation and Some New Methods for Their Study," California Institute of Technology, Rep E-115.1, 1965.

[2] Kling, C.L.,"A High Speed Photographic Study of Cavitation Bubble Collapse," Ph.D. thesis, University of Michigan, Ann Arbor, 1970.

[3] Blake, J.R. and Gibson, D.C., "Cavitation Bubbles Near Boundaries," Annual Review of Fluid Mechanics, vol. 19, pp. 99-123.

[4] Chahine, G. L., "Etude Locale du Phénomene de Cavitation Analyse des Facteurs Regissant la Dynamique des Interfaces," (Microscale study of cavitation. Analysis of factors controlling interface dynamics). Doctor ès Sciences Thesis, ENSTA, University Paris VI, 1979.

[5] Chahine, G. L., Duraiswami, R., "Boundary Element Method for Calculating 2D and 3D Underwater Explosion Bubble Behavior in Free Water and Near Structures," Naval Surface Warfare Center, Weapons Research and Technology Department, Report NSWCDD/TR-93/44, March 1994, (limited distribution).

[6] Snay, H. G. and Christian, E. A., "Underwater Explosion Phenomena: The Parameters of a Non-Migrating Bubble Oscillating in an Incompressible Medium," Navord Report 2437, Feb 1952.

[7] Cole, R. H., "Underwater Explosions," Dover Publications, 1948.

[8] Snay, H.G., "Model Tests and Scaling," NOLTR 63-257, 1964

[9] Goertner, J. F., "Vacuum Tank Studies of Gravity Migration of Underwater Explosion Bubbles," Navord Report 3902, Mar. 1956.

[10] Chahine, G. L., Duraiswami, R., and Kalumuck, K.M., "Boundary Element Method for Calculating 2-D and 3-D Underwater Explosion Loading on Nearby Structures Including Fluid Structure Interaction effects," Naval Surface Warfare Center, Weapons Research and Technology Department, Report NSWCDD/TR-93/46, expected Publication Nov. 1995, (limited distribution).

[11] Chahine, G. L. and Fruman, D. H., "Dilute Polymer Solution Effects on Bubble Growth and Collapse," Physics of Fluids, Vol., 22, No. 7, pp. 1406-1407, July 1979.
[12] Chahine, G. L. and Liu, H. L., "A Singular Perturbation Theory for the Growth of a Bubble Cluster in a Superheated Liquid," Journal of Fluid Mechanics, 156, pp. 257-279, July, 1985.
[13] Shepherd, J.E., "Interface Effects in Underwater Explosions," in "Conventional Weapons Underwater Explosions" ONR Workshop Report prepared by Georgia Institute of Technology, Dec.1988.
[14] Sternberg, H.M. and Walker, W.A., "Calculated Flow and Energy Distribution Following Underwater Detonation of Pentolite Sphere," Phys. Fluids 14, 1869-1878, 1971.
[15] Chahine, G. L., Kalumuck, K. M., "The Influence of Gas Diffusion on the Growth of a Bubble Cloud," ASME Cavitation and Multiphase Flow Forum 1987, pp. 17-21, June 1987.